Check for updates

Spurious proton transfer in hydrogen bonded dimers†

Joanatan Bautista-Renedo [iD] *[a] and Joel Ireta [iD] *[b]

In some hydrogen bonded systems, the proton may translocate along the hydrogen bond (hb) upon geometry optimization with electronic structure methods like density functional theory (DFT). Such proton transfer (pt) events, however, may be spurious. In this work, spurious pt events are investigated in a set of hydrogen bonded dimers formed with molecules HXN, where X stands for C, Si, Ge and Sn. It is found that standard approximations to the electronic exchange and correlation (xc) functional either predict spurious pt events or too strong hbs in all the $(HXN)_2$ dimers except the $(HCN)_2$ one. The latter result is revealed by comparing DFT calculations against wave function methods. Such spurious pt events may be avoided by fine-tuning the percentage of exact exchange (ex) in hybrid xc-functionals. It is shown that the minimum amount of ex to avoid a spurious pt event ranged from 8% to 90%, depending on the system, basis set and xc-functional approximation used. However, these fine-tuned xc-functionals inadequately describe the hb in the $(HXN)_2$ dimers. Moreover, it is determined that the spurious pt event originates from a wrong description of the isolated HXN molecules by xc-functionals that do not include ex or a small amount of it. Therefore, it is argued that one can determine if a pt event is spurious by analyzing the geometry and electronic structure of the isolated molecule.

1 Introduction

The hydrogen bond (hb), an interaction between an atom D (donor) and an atom or region A (acceptor) actuated by a H atom covalently bonded to D, influences decisively the properties of matter in which it occurs. The hb is also considered as a preliminary stage of a proton transfer (pt) reaction,[1,2] a crucial event involved in many chemical and biological processes.[3–6] Therefore, this fundamental interaction has been thoroughly investigated experimentally and theoretically to understand the physicochemical phenomena connected to its origin, and how it eases pt events. The theoretical procedures customarily used to investigate hydrogen bonded systems are electronic structure methods like second order Møller–Plesset perturbation theory (MP2), coupled clusters with singles, doubles and perturbative triple excitations (CCSD(T)),[7] and density functional theory (DFT) in its Kohn–Sham formulation.[8–10] CCSD(T) is considered the gold standard method for investigating hbs. MP2 is also considered to be a reliable method for studying hbs.

However, these methods are computationally very demanding, hence not suitable nowadays, to calculate very large systems (of hundreds or thousands of atoms) or systems modeled using periodic boundary conditions like solids or surfaces. DTF can be used to calculate the systems of such characteristics.[11–13] Moreover, depending on the approximation to the exchange and correlation (xc) functional used, DFT may adequately describe hydrogen bonded systems like peptides,[14–17] molecular crystals,[18–20] or catalytic materials,[21–24] *i.e.* complex systems whose physicochemical properties may be connected to hbs and pt events.

In the definition of a hb recommended by the international union of pure and applied chemistry,[25] the atom D is considered to be more electronegative than the H atom. Nevertheless, it has been shown experimentally and theoretically that hbs can be formed when D is less electronegative than H.[26] Investigating HXN dimers (Fig. 1), where X = C, Si, Ge, or Sn, with MP2 and CCSD(T), we have also found evidence for formation of hbs if D is less electronegative than H, as in $(HXN)_2$ where X = Si, Ge or Sn.[27] Unexpectedly, as shown in this work, DFT with standard xc-functionals predicts a spontaneous pt event in these dimers
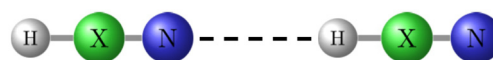
[a] Departamento de Química, División de Ciencias Básicas e Ingeniería, Universidad Autónoma Metropolitana-Iztapalapa, Ciudad de México 09340, Mexico.
E-mail: joanatan_br@xanum.uam.mx

[b] Departamento de Química, División de Ciencias Básicas e Ingeniería, Universidad Autónoma Metropolitana-Iztapalapa, Ciudad de México 09340, Mexico.
E-mail: iret@xanum.uam.mx

† Electronic supplementary information (ESI) available. See DOI: https://doi.org/10.1039/d4cp00907j

Fig. 1 Scheme of HXN dimers and their hydrogen bond (hb) interaction. X stands for C, Si, Ge or Sn.

upon geometry optimization, except for $(HCN)_2$, the case in which D is more electronegative than H, as in conventional hbs. Spurious pt events upon DFT geometry optimization have also been reported along with the formation of conventional hbs in organic crystals.[28] We wonder why standard approximations to the xc-functional fail to describe the hbs in $(HXN)_2$ when D is less electronegative than H and predict spurious pt events, and how to know that a pt event is spurious if CCSD(T) or MP2 calculations are not available.

DFT calculations may suffer from large inaccuracies related to the approximation to the xc-functional chosen,[29] e.g. it is known that xc-functionals that include generalized gradients of the electronic density (GGA) into their formulation, may lead to wrong predictions of pt barriers,[30] and spontaneous pt events.[28] It has been suggested that such false pt events are connected to the inability of current xc-functionals to correctly predict the linear dependence of the energy with respect to fractional electron numbers,[28,29,31,32] which triggers spurious delocalization of electrons or delocalized electrons with too low energies.[33] This electron delocalization error can be linked to the underestimation of reaction barriers and excitation energies and overestimations of binding energies in charge transfer complexes,[29] which may lead to incorrect identification of protonation sites, especially in acid–base multicomponent crystals.[28,34,35] In addition, it has been shown that the electron delocalization error can be reduced incorporating high percentages of exact exchange (ex) in the xc-functionals,[28,29,32,33,36,37] e.g. about 50% of ex is required for an accurate description of the energetics of charge transfer complexes, and about 40% to avoid spurious pt events in some molecular crystals.

In this work, the spurious pt events observed in the above mentioned HXN dimers are thoroughly investigated through DFT geometry optimizations. In order to do this, different approximations to the xc-functional are tested. It is shown that standard approximations to the xc-functional (GGAs, meta-GGAs, which include a dependence of the Laplacian of the density and/or the kinetic energy density, hybrid GGAs, with and without range separation and hybrid meta-GGAs) predict spurious pt events in these dimers. The tested functionals are the Perdew, Burke and Ernzerhof (PBE) GGA,[38] the strongly-constrained and appropriately normed (SCAN) meta-GGA[39–41] and its Laplacian-dependent deorbitalized variant (SCAN-L),[42] the Minnesota M06-L meta-GGA,[43] the PBE0 global hybrid functional, which have 25% of ex, and two versions of the Heyd–Scuseria–Ernzerhof range-separated hybrid functionals (HSE03 and HSE06),[44–48] which have 25% of ex at short range, the LC-PBE range-separated hybrid functional that includes 100% of ex at long range and the Minnesota M06-2X hybrid meta-GGA which includes 54% of ex.[49] Next, we gradually increase the ex contribution in PBE0 and the HSE family to find the amount of ex needed to avoid the pt in the investigated dimers. It is found that this amount is system and basis set dependent, however, beyond 44% of ex the pt is no longer observed in any of the investigated dimers. Additionally, it is shown that the maximum amount of xc needed to avoid pt increases as the short range in the HSE functional is reduced. Furthermore, we find that the amount of ex needed to avoid pt

does not guarantee an adequate description of hb properties like their strength (E_{hb}), i.e. the dimer association energy, the X–H vibrational frequencies ($\nu_{X–H}$) or the X$\cdots$H hb distance (d_{hb}). Lastly, we show that by analysing the local softness ($s(\mathbf{r})$), an intrinsic reactivity index that measures the capacity of the system to receive or donate electrons at a given molecular site,[50,51] and the magnitude of X–H bond distance ($d_{X–H}$), one can determine whether a spurious pt event is going to happen, even without performing a DFT calculation of the hydrogen bonded dimer, i.e. solely analyzing the monomer electronic structure and geometry. Furthermore, it is argued that these results give us insight into how the formation of a hb eases a proton transfer process, and about the ability of xc-functionals to describe non-conventional hbs.

2 Computational details

HXN monomers and dimers at angles of interaction of $180°$ are fully optimized using DFT with Grimme's-D3 dispersion correction[52] and the next set of xc-functionals: PBE, PBE0, LC-PBE, HSE03, HSE06, M06-L and M06-2X, while for SCAN and SCAN-L the Grimme's-D2 dispersion correction[53] is used as no D3 parameters for these functionals are implemented in the code used for the calculations. It is well known that Minnesota functionals are grid-sensitive, and for this reason, an extra-fine integration grid was used as well as for all the tested functionals.[54] This extra-fine grid assures a convergence in energy of $\sim 10^{-8}$ a.u.[55] We also calculate $(HXN)_2$, and its monomers, using MP2 with a frozen core and resolution of the identity approximations (RI-MP2) for comparison purposes. In all calculations the triple-zeta basis set of Ahlrichs with fuzzy functions def2-TZVPD,[56,57] the Dunning aug-cc-PVYZ basis sets with Y = D, T, and Q and the aug-cc-PVYZ-PP basis set for Sn are used.[58–60] Hereinafter, the latter basis set is solely referred to as aug-cc-PVYZ. The counterpoise method for correcting the basis set superposition error (BSSE) is used for calculating E_{hb}. Conformations with a distance A$\cdots$H shorter than X$\cdots$H upon geometry optimization are considered to result from a pt event. All electronic structure calculations and vibrational frequencies are carried out with the NWChem 6.8 code,[55] while the Multiwfn v3.8 program[61] is used for the analysis of properties related to the electron density. For geometry optimization calculations, it is considered that the structure has reached the minimum of the potential energy surface (PES) if the maximum and root mean square gradients are equal to or smaller than 1.5×10^{-5} and 1.0×10^{-5} in atomic units, respectively. Moreover, for the optimized structures obtained utilizing the def2-TZVPD basis set, it is confirmed that structures are at the minimum of PES corroborating the absence of imaginary frequencies.

It is worth mentioning that the implementation of HSE03 in the NWChem code, here denoted as $HSE03_{NW}$, is slightly different from the original HSE03. The separation between long and short range in the HSE functionals is controlled by the w parameter, whose values are $w = 0.11$ bohr^{-1} in HSE06, and $w = 0.15$ bohr^{-1} in HSE03. However, in NWChem $w = 0.33$ bohr^{-1} is used in $HSE03_{NW}$. As the larger the w value the smaller the short

This journal is © the Owner Societies 2024

Phys. Chem. Chem. Phys., 2024, 26, 21468–21475 | 21469

range, which is the section in which the ex is mixed with the GGA exchange, HSE03$_{NW}$ can be considered of ultra short range. We have tested both versions of the HSE03 functional. To determine the amount of ex to avoid pt we modify systematically the amount of ex in PBE0, HSE06, HSE03 and HSE03$_{NW}$. To avoid confusions, the functionals in which we modify the percentage of ex are renamed m-PBE0, m-HSE03, m-HSE03$_{NW}$ and m-HSE06.

To determine whether a pt could happen we calculate the quantity $s(\mathbf{r})$ (eqn (1)) for the HXN isolated monomers. Under finite differences and the rigid electronic band approach $s(\mathbf{r})$ can be estimated according to:[51,62,63]

$$s(\mathbf{r}) = \left(\frac{\partial\rho(\mathbf{r})}{\partial\mu}\right)_{\nu(\mathbf{r})} \approx \frac{1}{\Delta\mu}\int_{\mu_0}^{\mu_0+\Delta\mu} g(E,\mathbf{r})\mathrm{d}E \qquad (1)$$

where $\rho(\mathbf{r})$ is the electronic charge density, $\nu(\mathbf{r})$ is the external potential, $g(E,\mathbf{r})$ is the local density of states, μ is the chemical potential and $\Delta\mu$ is the change in μ with respect to the chemical potential of the unperturbed system μ_0. For finite gap systems, such as these investigated here, μ_0 is located at the middle between the edges of the conduction and valence bands. Usually, the $\Delta\mu$ value is chosen such that $s(\mathbf{r})$ integrates to -1 (for evaluating the capacity of donating electronic charge), or 1 (for evaluating the capacity of accepting electronic charge), which solely takes into account the highest and lowest energy orbitals contributing to the valence and conduction bands, respectively. However, we notice that in the HXN isolated monomers the occupied and empty orbitals pointing in the direction in which the hb is going to be formed, do not contribute either to the valence or the conduction bands. As our aim is to investigate if there is a correlation between the capacity of the HXN monomers to donate and accept charge along the direction in which the hb is going to be formed, and an eventual pt event, the $\Delta\mu$ used for evaluating $s(\mathbf{r})$ is chosen such that the first occupied and virtual orbitals lying along the hb forming direction are taken into account in the $s(\mathbf{r})$ calculation.

Although $s(\mathbf{r})$ is usually applied for elucidating the reactivity of organic molecules, proteins and surfaces,[51,64–67] it has also being correlated with the ability of a chemical group to form hbs,[23] and here we show that it can help to elucidate whether a pt could occur upon geometry optimization, without carrying the geometry optimization.

3 Results

In Tables 1 and 2 are listed the d_{hb} and E_{hb} values obtained with the tested xc-functionals and the aug-cc-PVQZ and def2-TZVPD basis sets. The results obtained with aug-cc-PVDZ and aug-cc-PVTZ are listed in Tables S1 and S2 of the ESI.† For comparison purposes, values obtained with MP2 and RI-MP2 are also listed along with those reported in ref. 27 calculated with MP2 and CCSD(T) at the complete basis set extrapolation (CBS). First, we notice that all xc-functionals together with the dispersion correction and any of the basis sets used predict no pt events in (HCN)$_2$, the dimer in which D is more electronegative than

Table 1 Hydrogen bond distance, d_{hb} (in Å) and hydrogen bond strength, E_{hb} (in kcal mol^{-1}), in (HCN)$_2$

Method[a]	aug-cc-PVQZ		def2-TZVPD	
	d_{hb}	E_{hb}	d_{hb}	E_{hb}
PBE-D3	2.18	−4.83	2.21	−4.83
SCAN-D2	2.19	−5.52	2.20	−4.07
SCAN-L-D2	2.13	−5.70	2.13	−4.74
M06-L-D3	2.17	−4.01	2.16	−4.23
PBE0-D3	2.18	−4.98	2.19	−4.98
PBE0	2.19	−4.59	2.23	−4.60
HSE03-D3	2.22	−4.69	2.23	−4.69
HSE03$_{NW}$-D3	2.20	−4.81	2.23	−4.81
HSE06-D3	2.22	−4.68	2.23	−4.68
LC-PBE-D3	2.06	−6.08	2.07	−6.16
M06-2X-D3	2.21	−4.52	2.24	−4.45
MP2	2.19	−4.80		
RI-MP2			2.22	−4.59
MP2/CBS[b]	2.15[c]	−4.88		
CCSD(T)/CBS[d]		−4.68		

[a] Energies are basis set superposition error corrected. [b] Complete basis set extrapolation (CBS) of MP2 single point calculations on MP2/aug-cc-pVDZ optimized geometries. Results from ref. 27. [c] MP2/aug-cc-pVDZ optimized geometries. [d] CBS of CCSD(T) single point calculations on MP2/aug-cc-pVDZ optimized geometries. Results from ref. 27

H. This result is in accordance with the MP2 and RI-MP2 results (Table 1 and Table S1 in the ESI†). For the other dimers (Table 1 and Tables S1 and S2 in the ESI†) where D is less electronegative than H, pt events may be obtained upon geometry optimization depending on the functional and/or basis set used. For example, for (HSiN)$_2$ PBE-D3 and SCAN-L-D2 predict a pt event disregarding the basis set utilized, however SCAN-D2 predicts a pt event only if the aug-cc-PVDZ basis set is used. Similarly, for (HGeN)$_2$, PBE-D3 and SCAN-L-D2 predict pt events independently of the basis set used, as well as SCAN-D2 with all the basis sets but the aug-cc-PVTZ. For (HSnN)$_2$ all the combinations of xc-functional/basis-set predict pt events, except if the M06-2X-D3 xc-functional is used with any of the basis sets or LC-PBE-D3 with aug-cc-PVQZ or def2-TZVPD. Nevertheless, MP2 and RI-MP2 predict no pt events for the investigated dimers independently of the basis set used.

The d_{hb} and E_{hb} values obtained using either def2-TZVPD or aug-cc-PVQZ basis sets and any of the tested functionals differ little between them, except if these basis sets are utilized together with the SCAN-D3 or SCAN-L-D2 xc-functionals. The latter combinations lead to differences between 1 and 3 kcal mol^{-1} for E_{hb}. Although differences in d_{hb} are small, 0.06 Å at most (Tables 1 and 2). Yet, the results obtained with these two basis sets are consistent regarding the prediction of pt events. The other basis sets, aug-cc-PVDZ and aug-cc-PVTZ, give somewhat erratic results concerning pt events, particularly if these are used together with the SCAN-D2 or the LC-PBE-D3 xc-functionals. Hereinafter we use primarily the def2-TZVPD basis sets and solely key results are corroborated repeating the calculations using the aug-cc-PVQZ basis set.

The def2-TZVPD basis set together with the tested xc-functionals describe adequately the hb in (HCN)$_2$, within an error bar of 0.6 kcal mol^{-1} with respect to CCSD(T)/CBS for the hb strength, and of 0.1 Å with respect to MP2/aug-cc-pVDZ results for d_{hb},

21470 | *Phys. Chem. Chem. Phys.*, 2024, **26**, 21468–21475

This journal is © the Owner Societies 2024

Table 2 Hydrogen bond distance, d_{hb} (in Å), and strength, E_{hb} (in kcal mol^{-1}), in $(HXN)_2$ dimers with X = Si, Ge, and Sn

System/method[a]	aug-cc-PVQZ		def2-TZVPD	
	d_{hb}	E_{hb}[b]	d_{hb}	E_{hb}[b]
$(HSiN)_2$				
PBE-D3		–pt–		–pt–
SCAN-D2	1.85	−7.90	1.91	−5.09
SCAN-L-D2		–pt–		–pt–
M06-L-D3	2.07	−5.06	2.10	−5.18
PBE0-D3	1.95	−7.00	1.96	−7.11
PBE0	1.96	−6.41	1.98	−6.41
HSE03-D3	2.01	−6.36	2.02	−6.31
HSE03$_{NW}$-D3	1.92	−6.44	1.94	−6.56
HSE06-D3	2.01	−6.37	2.03	−6.48
LC-PBE-D3	1.82	−9.59	1.84	−9.72
M06-2X-D3	2.08	−6.79	2.12	−7.10
MP2	2.22	−3.75		
RI-MP2			2.29	−3.40
MP2/CBS[c]	2.21[d]	−3.68		
CCSD(T)/CBS[e]		−4.97		
$(HGeN)_2$				
PBE-D3		–pt–		–pt–
SCAN-D2		–pt–		–pt–
SCAN-L-D2		–pt–		–pt–
M06-L-D3	2.02	−4.75	2.03	−5.46
PBE0-D3	1.91	−6.64	1.93	−6.87
PBE0	1.93	−5.94	1.95	−5.99
HSE03-D3	1.97	−5.99	1.99	−5.92
HSE03$_{NW}$-D3	1.85	−6.13	1.88	−6.35
HSE06-D3	1.98	−6.00	2.00	−6.25
LC-PBE-D3	1.82	−9.21	1.85	−9.51
M06-2X-D3	2.10	−6.32	2.13	−6.75
MP2	2.01	−3.18		
RI-MP2			2.21	−3.03
MP2/CBS[c]	2.09[d]	−3.58		
CCSD(T)/CBS[e]		−4.91		
$(HSnN)_2$				
PBE-D3		–pt–		–pt–
SCAN-D2		–pt–		–pt–
SCAN-L-D2		–pt–		–pt–
M06-L-D3		–pt–		–pt–
PBE0-D3		–pt–		–pt–
PBE0		–pt–		–pt–
HSE03-D3		–pt–		–pt–
HSE03$_{NW}$-D3		–pt–		–pt–
HSE06-D3		–pt–		–pt–
LC-PBE-D3	1.65	−9.17	1.71	−9.04
M06-2X-D3	2.00	−5.72	2.11	−5.46
MP2	1.70	−2.11		
RI-MP2			2.10	−3.04
MP2/CBS[c]	1.91[d]	−3.49		
CCSD(T)/CBS[e]		−2.67		

[a] Basis set superposition error corrected values obtained using the def2-TZVPD basis set. [b] pt stands for proton transfer. [c] Complete basis set extrapolation (CBS) of MP2 single point calculations on MP2/aug-cc-pVDZ optimized geometries. Results from ref. 27. [d] MP2/aug-cc-pVDZ optimized geometries. Results from ref. 27. [e] CBS of CCSD(T) single point calculations on MP2/aug-cc-pVDZ optimized geometries. Results from ref. 27.

the three dimers, SCAN-D3 in two ($(HGeN)_2$ and $(HSnN)_2$), and M06-L-D3 in one ($(HSnN)_2$). Hybrid xc-functionals together with the D3 dispersion correction predict either too strong hbs, with error bars larger than 1.3 kcal mol^{-1}, as in $(HSiN)_2$ and $(HGeN)_2$, or pt events, as in $(HSnN)_2$, except for LC-PBE-D3 that does not predict pt events in any case. Yet, the largest deviations from the CCSD(T)/CBS E_{hb} values are obtained with LC-PBE-D3. These deviations lead to errors in the order of the expected values. The hybrid meta-GGA M06-2X together with the dispersion correction D3 also predicts no pt events, however, it greatly overestimates the hb strength with errors that can even be of the same magnitude as the E_{hb} value obtained with CCSD(T)/CBS. For MP2 the description of these hbs in which D is less electronegative than H is also challenging. The MP2/aug-cc-PVQZ error can be as large as 1.7 kcal mol^{-1}, with respect to CCSD(T), in the calculations of E_{hb}. This error may increase in some dimers if RI-MP2/def2-TZVPD is used, e.g. for $(HGeN)_2$ it amounts to 1.88 kcal mol^{-1}. Still, neither MP2 nor RI-MP2 predict pt events.

According to the previous results only hybrid functionals with ex larger than 50% (LC-PBE and M06-2X) do not predict any spurious pt events in the investigated dimers. However, these functionals greatly overestimate the E_{hb}. To determine the minimum amount of ex that is required to avoid spurious pt events, we have systematically modified the percentage of ex in PBE0, HSE03, HSE03$_{NW}$ and HSE06 (see Fig. S1 in the ESI†). It is found that the minimum amount of ex to avoid pt is system dependent, e.g. for $(HSiN)_2$ and $(HGeN)_2$ less than 10% of ex in m-HSE06, m-PBE0 and m-HSE03, and between 13% and 15% in m-HSE03$_{NW}$ is required (see Table 3). However, that amount increases significantly for $(HSnN)_2$, between 40% and 44% in m-HSE06, m-PBE0 and m-HSE03, and up to 90% in m-HSE03$_{NW}$. In all these cases, m-HSE03$_{NW}$ requires the largest amount of ex to avoid the pt event. This result suggest that for range separated xc-functionals the smaller the short range the larger the ex needed to avoid the pt. Yet, E_{hb} is overestimated using the xc-functionals modified with the minimum amount of ex listed in Table 3, and d_{hb} is

Table 3 Minimum amount of exact exchange, ex, to avoid proton transfer and the hydrogen bonding distance, d_{hb} (in Å), and strength, E_{hb} (in kcal mol^{-1}) predicted with that amount of ex

System	Method[a]	% ex	d_{hb}	E_{hb}
$(HSiN)_2$	m-HSE06-D3	7(7)	1.79(1.76)	−6.43(−6.49)
	m-HSE03-D3	8	1.81	−6.42
	m-HSE03$_{NW}$-D3	13	1.75	−6.47
	m-PBE0	8	1.80	−6.06
$(HGeN)_2$	m-HSE06-D3	7(9)	1.69(1.75)	−6.13(−6.17)
	m-HSE03-D3	8	1.72	−6.12
	m-HSE03$_{NW}$-D3	15	1.74	−6.14
	m-PBE0	8	1.75	−5.66
$(HSnN)_2$	m-HSE06-D3	40(44)	1.90(1.88)	−5.38(−5.51)
	m-HSE03-D3	44	1.91	−5.36
	m-HSE03$_{NW}$ -D3	90	2.01	−5.49
	m-PBE0	43	1.81	−5.70

[a] Data in parenthesis are obtained with the aug-cc-PVQZ basis set. The E_{hb} values are basis set superposition error corrected.

except for LC-PBE-D3 that predicts a too strong hb, with $E_{hb} \sim$ 1.5 kcal mol^{-1} larger than the CCSD(T)/CBS result. For the other dimers ($(HXN)_2$ where X = Si, Ge or Sn), however, the GGA PBE-D3 predicts pt events. The meta-GGAs-D3 either predict E_{hb} within an error bar of 0.6 kcal mol^{-1} and d_{hb} within an error bar of 0.3 Å, or pt events; i.e. SCAN-L-D3 predicts pt events in

underestimated. Increasing the amount of ex can improve the prediction of E_{hb} solely with the m-HSE03 functional, and with the other functionals the overestimation is increased. Nevertheless, the description of d_{hb} will be improved with any of the xc-functionals tested if ex is increased (see Fig. S1 in the ESI†), except in $(HSnN)_2$ calculated with m-HSE03 or m-HSE03$_{NW}$. For that system, the d_{hb} values obtained with the minimum amount of ex required to avoid pt, is already quite close to the one obtained with MP2. The amount of ex to avoid spurious pt events is also basis set dependent, although only slightly, *e.g.* the amount of ex increases between 1% and 4% if the calculations are performed with aug-cc-PVQZ instead of def2-TZVPD (Table 3).

Analyzing the description of the optimized HXN isolated-molecules obtained with different amounts of ex, we find that the d_{X-H} (Table 4 and Table S3 in the ESI†) and the ν_{X-H} (Table S4 in ESI†) values deviate significantly from the corresponding MP2 values if no ex is included, as when using PBE. For example, PBE predicts d_{X-H} to be between 0.7% and 2.9% longer than the MP2 values, and between 2.8% and 12.4% smaller ν_{X-H} frequencies than the MP2 ones. Increasing ex, the overestimation of d_{X-H} and the underestimation of ν_{X-H} by DFT may even turn into underestimation and overestimation, respectively, as

when ex is increased beyond 40%. The d_{X-H} and ν_{X-H} values are somewhat indicative of how strong is the proton bonded to the X atom. Thus, the latter results suggest that the proton in the HXN molecules becomes more labile as the amount of ex included in the xc-functional is reduced, hence more prone to be transferred upon hydrogen bonding. Therefore, it seems that the spurious pt event in $(HXN)_2$ predicted by DFT is partly connected to an inadequate description of the X–H bond in the isolated HXN molecules when no ex, or a small amount of it, is included in the xc-functional. That is, to the prediction by DFT of longer X–H covalent bonds and smaller ν_{X-H} frequencies than the expected ones, particularly for the monomers in which X is less electronegative than H.

It may be then possible to determine if a pt event is spurious by analyzing the isolate molecule, *i.e.*, before hydrogen bonding. For example, if the deviation of d_{X-H} with respect to the MP2 result is larger than 1.3% a pt event will happen upon hydrogen bonding, and if such deviation is smaller than 0.7% it will not (see Table S3 in the ESI†). However, if the deviation is between 1.3% and 0.7%, the outcome cannot be predicted. A similar conclusion can be reached analyzing the deviations of ν_{X-H} from the MP2 values; *i.e.*, if the deviation $\leq -6\%$ a pt event will happen, and if the deviation $\geq -2.5\%$ it will not. Still, for some deviation intervals one cannot predict if the pt event will happen or not.

As the formation of a hb will tend to affect the strength of the X–H bond in the HXN molecules, likely due to a redistribution of the charge density upon hydrogen bonding, one may wonder if there is a correlation between the capacity of the N atom and that of the X–H bond, in the isolated molecule, to donate/accept charge, respectively, and an eventual pt event. The latter because the acceptor atom's capacity to donate charge has been correlated with its ability to form a hydrogen bond.[23] Thus, we have estimated the capacity of the isolated HXN (monomer) to donate/accept electronic charge by means of $s(\mathbf{r})$. The donating capacity, $(s(\mathbf{r})^-)$, is calculated considering the highest-energy occupied-orbitals, at the N atom, pointing along the direction of the hb formation. For calculating the accepting capacity, $(s(\mathbf{r})^+)$ are considered the lowest-energy empty-orbitals, at the X–H bond, pointing along the direction of the hb formation (Fig. 2). For comparison purposes $\Delta\mu > 0$ is considered in the calculation of both $s(\mathbf{r})^-$ and $s(\mathbf{r})^+$. We estimate how much electronic charge could transfer in the process of the formation of the hb overlapping $s(\mathbf{r})^-$ with $s(\mathbf{r})^+$. For that, we plot together $s(\mathbf{r})^-$ and $s(\mathbf{r})^+$ at HXN (upper part of Fig. 2). Next, two replicas are made and located one to the left and one to the right as depicted in the lower part of Fig. 2. The origin of the combined plot is at the N atom of the molecule located to the left. The molecule to the right is located in a position such that its H atom is at the distance $d_{N\cdots H} = 0.68(r_N + r_H)$ from the origin of the combined plots r_N and r_H stand for the van der Waals radius of N and H, respectively. These van der Waals radius are determined integrating the electronic density obtained from a DFT calculation with the corresponding percentage of ex. For each case, the van der Waals radius is considered to be the radius of the sphere in which the electronic density integrates to the 99.9% of the value it should
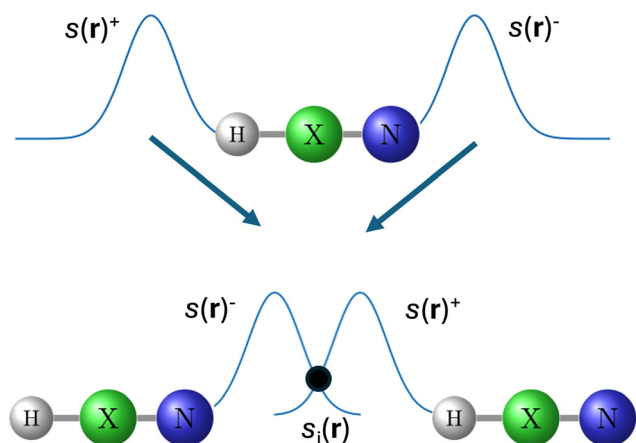
Table 4 Value of the softness at the intersection point, $s_i(\mathbf{r})$ in Å^{-3} eV^{-1}, the bond distance, d_{X-H} in Å, in the monomers and the proton lability index, L in Å^{-2} eV^{-1}

System	% ex[a]	$s_i(\mathbf{r})$	d_{X-H}	L
HCN	0	0.047(0.035)	1.076(1.075)	5.1(3.8)
	10	0.038	1.073	4.1
	20	0.031	1.070	3.3
	25	(0.02)	(1.068)	(2.1)
	40	0.022	1.065	2.3
	50	(0.012)	(1.061)	(1.3)
	100	0.005	1.068	0.0
HSiN	0	0.063(0.065)	1.504(1.502)	9.5(9.8)
	10	0.058	1.497	8.7
	20	0.053	1.491	7.9
	25	(0.052)	(1.486)	(7.7)
	40	0.045	1.479	6.7
	50	(0.043)	(1.473)	(6.3)
	100	0.008	1.488	0.0
HGeN	0	0.064(0.064)	1.538 (1.535)	9.8(9.8)
	10	0.060	1.530	9.2
	20	0.055	1.525	8.4
	25	(0.055)	(1.519)	(8.4)
	40	0.048	1.513	7.3
	50	(0.045)	(1.506)	(6.8)
	100	0.011	1.519	0.0
HSnN	0	0.068(0.062)	1.703(1.703)	11.6 (10.6)
	10	0.062	1.695	10.5
	20	0.057	1.688	9.6
	25	(0.056)	(1.686)	(9.4)
	40	0.050	1.676	8.4
	50	(0.044)	(1.672)	(7.4)
	100	0.016	1.655	0.0

[a] 0% and 100% of ex correspond to calculations with PBE and MP2, respectively. Otherwise, m-HSE06-D3 is used. The def2-TZVPD basis set is used in these calculations, except for the data in parenthesis, which are obtained with the aug-cc-PVQZ basis set.

21472 | *Phys. Chem. Chem. Phys.*, 2024, **26**, 21468–21475

This journal is © the Owner Societies 2024

Fig. 2 Upper scheme, local softness $s(\mathbf{r})^-$ (donating capacity) and $s(\mathbf{r})^+$ (accepting capacity) at the HXN isolated molecule. Lower scheme, replicas of the HXN isolated molecule located at the distance $d_{N\cdots H}$ in which $s(\mathbf{r})^-$ and $s(\mathbf{r})^+$ overlap. Considering the origin at the N atom to the left, $d_{N\cdots H}$ is calculated as $d_{N\cdots H} = 0.68(r_N + r_H)$, where r_N and r_H stand for the van der Waals radius of N and H, respectively. $s_i(\mathbf{r})$ stands for the value in which $s(\mathbf{r})^- = s(\mathbf{r})^+$. X stands for C, Si, Ge or Sn.

integrate in an infinite sphere. In such arrangement, the tails of $s(\mathbf{r})^-$ and $s(\mathbf{r})^+$ overlap (see Fig. S2 in ESI†). The values of $s(\mathbf{r})$ at the intersecting point ($s_i(\mathbf{r})$, Fig. 2) are listed in Table 4. This value reduces as the percentage of ex is increased. We find that if $s_i(\mathbf{r})$ is larger than 0.060 (in units of $\text{Å}^{-3}\,\text{eV}^{-1}$) a spurious pt event will happen upon hydrogen bonding, and if it is lower or equal to 0.05 it will not. However, if $s_i(\mathbf{r})$ is between 0.06 and 0.05 it cannot be predicted whether a spurious pt event will happen or not. We note that combining $s_i(\mathbf{r})$ and d_{X-H} we can identify all the spurious pt events; *i.e.*, we find that if the quantity $L = s_i(\mathbf{r})d_{X-H} \times 100$, here called the lability index, is larger than 9.2 (in units of $\text{Å}^{-2}\,\text{eV}^{-1}$) a spurious pt event will be observed, at least in the systems investigated here (see Table 4). It is worth mentioning that L calculated with MP2 is ~ 0.0 for all the systems, which suggests that when fully considering the ex the possibility of a pt event upon hydrogen bonding practically vanishes, in the systems investigated here. Moreover if the lability index is calculated with the aug-cc-PVQZ basis sets (see Table 4) the same conclusion is reached.

4 Discussion

In DFT calculations, one may usually associate a spurious pt event in hydrogen bonded systems with a bad description of the hb by the xc-functional. This bad description may be due to the charge delocalization error common to many of the current xc-functionals. The results presented above, however, reveal that spurious pt events may actually be connected to a bad description of the X–H bond in the non-hydrogen bonded monomer by the xc-functional, particularly when X is more electronegative than H, and not to the nature of the hb formed; *i.e.*, conventional or not conventional. The latter is corroborated calculating L, that depends only on quantities obtained from the isolated, non-hydrogen bonded, molecules. This empirical index combines a

parameter connected to the strength of the X–H bond (d_{X-H}), and an estimation of how much charge could be transferred upon hydrogen bonding ($s_i(\mathbf{r})$), a quantity that depends on the charge donor/acceptor capabilities of the isolated molecule. Thus, it seems that for no ex or a small amount of it considered in the xc-functional, the X–H may be predicted to be too elongated (*i.e.* weakened) and with an enhanced capability for accepting charge, that together with a great ability for donating charge of the N atom predicted with a given xc-functional, combine to ease the pt event upon hydrogen bonding. All these characteristics diminish as the percentage ex included in the xc-functional is increased, up to a point in which the pt event is no longer feasible. Nevertheless, preventing the pt event by increasing the percentage of ex tends to deteriorate the description of the hb.

5 Conclusions

Studying the proton translocation along the hb through geometry optimization with DFT, we find that the amount of ex required to avoid a spurious pt event in the $(HXN)_2$ dimers is system, basis set and xc-functional approximation dependent. Also, it is demonstrated that the spurious pt event is connected to an inadequate description of the isolated HXN molecule by a given xc-functional, not to the type of the hb that is expected to be formed. Once the description of the isolated molecule is improved by increasing the amount of ex included in the xc-functional, the spurious pt event is avoided. Still, even though the pt transfer is avoided, the hb may not be well described by the xc-functional. Our results may help to elucidate whether a pt event is spurious or not in DFT studies of more complex systems.

Data availability

The data supporting this article have been included as part of the ESI.†

Conflicts of interest

There are no conflicts to declare.

Acknowledgements

Notes and references

1 T. Steiner, *Angew. Chem., Int. Ed.*, 2002, **41**, 48–76.
2 S. J. Grabowski, *Molecules*, 2020, **25**, 4668.
3 S. Hammes-Schiffer, *J. Phys. Chem. B*, 2021, **125**, 3725–3726.
4 I. Belevich, M. Verkhovsky and M. Wikstrom, *Nature*, 2006, **440**, 829–832.

This journal is © the Owner Societies 2024

Phys. Chem. Chem. Phys., 2024, **26**, 21468–21475 | **21473**

5   S. Adam and A.-N. Bondar, *PLoS One*, 2018, **13**, 1–28.

6   H. Ishikita and K. Saito, *J. R. Soc., Interface*, 2014, **11**, 20130518.

7   R. Sedlak, T. Janowski, M. Pitonak, J. Rezac, P. Pulay and P. Hobza, *J. Chem. Theory Comput.*, 2013, **9**, 3364–3374.

8   C. Tuma, A. Boese and N. Handy, *Phys. Chem. Chem. Phys.*, 1999, **1**, 3939–3947.

9   J. Ireta, J. Neugebauer and M. Scheffler, *J. Phys. Chem. A*, 2004, **108**, 5692–5698.

10 Y. Zhao and D. Truhlar, *J. Chem. Theory Comput.*, 2005, **1**, 415–432.

11 J. C. A. Prentice, J. Aarons, J. C. Womack, A. E. A. Allen, L. Andrinopoulos, L. Anton, R. A. Bell, A. Bhandari, G. A. Bramley, R. J. Charlton, R. J. Clements, D. J. Cole, G. Constantinescu, F. Corsetti, S. M.-M. Dubois, K. K. B. Duff, J. M. Escartn, A. Greco, Q. Hill, L. P. Lee, E. Linscott, D. D. O'Regan, M. J. S. Phipps, L. E. Ratcliff, A. R. Serrano, E. W. Tait, G. Teobaldi, V. Vitale, N. Yeung, T. J. Zuehlsdorff, J. Dziedzic, P. D. Haynes, N. D. M. Hine, A. A. Mostofi, M. C. Payne and C.-K. Skylaris, *J. Chem. Phys.*, 2020, **152**, 174111.

12 W. Dawson, A. Degomme, M. Stella, T. Nakajima, L. E. Ratcliff and L. Genovese, *Wiley Interdiscip. Rev.: Comput. Mol. Sci.*, 2022, **12**, e1574.

13 A. Nakata, J. S. Baker, S. Y. Mujahed, J. T. L. Poulton, S. Arapan, J. Lin, Z. Raza, S. Yadav, L. Truflandier, T. Miyazaki and D. R. Bowler, *J. Chem. Phys.*, 2020, **152**, 164112.

14 L. Ismer, J. Ireta, S. Boeck and J. Neugebauer, *Phys. Rev. E*, 2005, **71**, 031911.

15 L. Ismer, J. Ireta and J. Neugebauer, *J. Phys. Chem. B*, 2008, **112**, 4109–4112.

16 J. Nochebuena, A. Ramirez and J. Ireta, *Int. J. Quantum Chem.*, 2015, **115**, 1613–1620.

17 J. Ireta, *Int. J. Quantum Chem.*, 2012, **112**, 3612–3617.

18 M. Neumann and M. Perrin, *J. Phys. Chem. B*, 2005, **109**, 15531–15541.

19 J. M. del Campo and J. Ireta, *Phys. Chem. Chem. Phys.*, 2021, **23**, 11931–11936.

20 N. E. Gonzalez-Diaz, R. Lopez-Rendon and J. Ireta, *J. Phys. Chem. C*, 2019, **123**, 2526–2532.

21 J. K. Norskov, F. Abild-Pedersen, F. Studt and T. Bligaard, *Proc. Natl. Acad. Sci. U. S. A.*, 2011, **108**, 937–943.

22 C. Cuautli, J. S. Valente, J. C. Conesa, M. V. Ganduglia-Pirovano and J. Ireta, *J. Phys. Chem. C*, 2019, **123**, 8777–8784.

23 G. Castro, J. S. Valente, M. Galvan and J. Ireta, *Phys. Chem. Chem. Phys.*, 2022, **24**, 23507–23516.

24 J. Ireta, F. Aparicio, M. Viniegra and M. Galvan, *J. Phys. Chem. B*, 2003, **107**, 811–818.

25 E. Arunan, G. R. Desiraju, R. A. Klein, J. Sadlej, S. Scheiner, I. Alkorta, D. C. Clary, R. H. Crabtree, J. J. Dannenberg, P. Hobza, H. G. Kjaergaard, A. C. Legon, B. Mennucci and D. J. Nesbitt, *Pure Appl. Chem.*, 2011, **83**, 1637–1641.

26 S. Civis, M. Lamanec, V. Spirko, J. Kubista, M. Spet'ko and P. Hobza, *J. Am. Chem. Soc.*, 2023, **145**, 8550–8559.

27 J. M. Bautista-Renedo, H. Reyes-Pérez, E. Cuevas-Yañez, C. Barrera-Díaz, N. González-Rivas and J. Ireta, *RSC Adv.*, 2019, **9**, 5937–5941.

28 L. M. LeBlanc, S. G. Dale, C. R. Taylor, A. D. Becke, G. M. Day and E. R. Johnson, *Angew. Chem., Int. Ed.*, 2018, **57**, 14906–14910.

29 A. J. Cohen, P. Mori-Sanchez and W. Yang, *Science*, 2008, **321**, 792–794.

30 G. F. Mangiatordi, E. Bremond and C. Adamo, *J. Chem. Theory Comput.*, 2012, **8**, 3082–3088.

31 D. Flait and M. Head-Gordon, *J. Phys. Chem. Lett.*, 2018, **9**, 6280–6288.

32 K. R. Bryenton, A. A. Adeleke, S. G. Dale and E. R. Johnson, *Wiley Interdiscip. Rev.: Comput. Mol. Sci.*, 2022, **13**, e1631.

33 X. Zheng, M. Liu, E. R. Johnson, J. Contreras-García and W. Yang, *J. Chem. Phys.*, 2012, **137**, 214106.

34 J. Blahut, J. R. Stocek, M. Sala and M. Dracinsky, *J. Magn. Reson.*, 2022, **345**, 107334.

35 M. Husak, S. Sajbanova, J. Klimes and A. Jegorovc, *Acta Crystallogr., B: Struct. Sci., Cryst. Eng. Mater.*, 2022, **78**, 781–788.

36 J. S. Stevens, S. J. Byard, C. C. Seaton, G. Sadiq, R. J. Davey and S. L. M. Schroeder, *Phys. Chem. Chem. Phys.*, 2014, **16**, 1150–1160.

37 B. G. Janesko, *Chem. Soc. Rev.*, 2021, **50**, 8470–8495.

38 J. P. Perdew, K. Burke and M. Ernzerhof, *Phys. Rev. Lett.*, 1996, **77**, 3865.

39 J. Sun, A. Ruzsinszky and J. P. Perdew, *Phys. Rev. Lett.*, 2015, **115**, 036402.

40 J. Cirera and E. Ruiz, *J. Phys. Chem.*, 2020, **124**, 5053–5058.

41 J. Sun, A. Ruzsinszky and J. P. Perdew, *Phys. Rev. Lett.*, 2015, **115**, 036402.

42 D. Mejia-Rodriguez and S. B. Trickey, *Phys. Rev. A*, 2017, **96**, 052512.

43 Y. Wang, X. Jin, H. S. Yu, D. G. Truhlar and X. He, *Proc. Natl. Acad. Sci. U. S. A.*, 2017, **114**, 8487–8492.

44 J. Heyd, G. E. Scuseria and M. Ernzerhof, *J. Chem. Phys.*, 2003, **118**, 8207–8215.

45 J. Heyd, G. E. Scuseria and M. Ernzerhof, *J. Chem. Phys.*, 2006, **124**, 21996.

46 J. Heyd and G. E. Scuseria, *J. Chem. Phys.*, 2004, **121**, 1187–1192.

47 J. Heyd and G. E. Scuseria, *J. Chem. Phys.*, 2004, **120**, 7274–7280.

48 J. Heyd, J. E. Peralta, G. E. Scuseria and R. L. Martin, *J. Chem. Phys.*, 2005, **123**, 174101.

49 Y. Zhao and D. G. Truhlar, *Theor. Chem. Acc.*, 2008, **120**, 215–241.

50 W. Yang and R. G. Parr, *Proc. Natl. Acad. Sci. U. S. A.*, 1985, **82**, 6723–6726.

51 K. D. Brommer, M. Galvan, A. Dal Pino Jr and J. Joannopoulos, *Surf. Sci.*, 1994, **314**, 57–70.

52 S. Grimme, J. Antony, S. Ehrlich and H. Krieg, *J. Chem. Phys.*, 2010, **132**, 154104.

53 S. Grimme, *J. Comput. Chem.*, 2006, **27**, 1787–1799.

54 S. Dasgupta and J. M. Herbert, *J. Comput. Chem.*, 2017, **38**, 869–882.

55 E. Aprà, E. J. Bylaska, W. A. de Jong, N. Govind, K. Kowalski, T. P. Straatsma, M. Valiev, H. J. J. van Dam, Y. Alexeev, J. Anchell, V. Anisimov, F. W. Aquino, R. Atta-Fynn, J. Autschbach, N. P. Bauman, J. C. Becca, D. E. Bernholdt, K. Bhaskaran-Nair, S. Bogatko, P. Borowski, J. Boschen,

21474 | *Phys. Chem. Chem. Phys.*, 2024, **26**, 21468–21475

This journal is © the Owner Societies 2024

J. Brabec, A. Brunauer, E. Cauët, Y. Chen, G. N. Chuev, C. J. Cramer, J. Daily, M. J. O. Deegan, T. H. Dunning Jr., M. Dupuis, K. G. Dyall, G. I. Fann, S. A. Fischer, A. Fonari, H. Früchtl, L. Gagliardi, J. Garza, N. Gawande, S. Ghosh, K. Glaesemann, A. W. Götz, J. Hammond, V. Helms, E. D. Hermes, K. Hirao, S. Hirata, M. Jacquelin, L. Jensen, B. G. Johnson, H. Jónsson, R. A. Kendall, M. Klemm, R. Kobayashi, V. Konkov, S. Krishnamoorthy, M. Krishnan, Z. Lin, R. D. Lins, R. J. Littlefield, A. J. Logsdail, K. Lopata, W. Ma, A. V. Marenich, J. Martin del Campo, D. Mejia-Rodriguez, J. E. Moore, J. M. Mullin, T. Nakajima, D. R. Nascimento, J. A. Nichols, P. J. Nichols, J. Nieplocha, A. Otero-de-la Roza, B. Palmer, A. Panyala, T. Pirojsirikul, B. Peng, R. Peverati, J. Pittner, L. Pollack, R. M. Richard, P. Sadayappan, G. C. Schatz, W. A. Shelton, D. W. Silverstein, D. M. A. Smith, T. A. Soares, D. Song, M. Swart, H. L. Taylor, G. S. Thomas, V. Tipparaju, D. G. Truhlar, K. Tsemekhman, T. Van Voorhis, A. Vázquez-Mayagoitia, P. Verma, O. Villa, A. Vishnu, K. D. Vogiatzis, D. Wang, J. H. Weare, M. J. Williamson, T. L. Windus, K. Wolinski, A. T. Wong, Q. Wu, C. Yang, Q. Yu, M. Zacharias, Z. Zhang, Y. Zhao and R. J. Harrison, *J. Chem. Phys.*, 2020, **152**, 184102.

56 F. Weigend and R. Ahlrichs, *Phys. Chem. Chem. Phys.*, 2005, **7**, 3297–3305.

57 F. Weigend, *Phys. Chem. Chem. Phys.*, 2006, **8**, 1057–1065.

58 J. Dunning and H. Thom, *J. Chem. Phys.*, 1989, **90**, 1007–1023.

59 R. A. Kendall, J. Dunning, H. Thom and R. J. Harrison, *J. Chem. Phys.*, 1992, **96**, 6796–6806.

60 K. A. Peterson, *J. Chem. Phys.*, 2003, **119**, 11099–11112.

61 T. Lu and F. Chen, *J. Comput. Chem.*, 2012, **33**, 580–592.

62 L. I. Perea-Ramírez, A. Guevara-García and M. Galván, *J. Mol. Model.*, 2018, **24**, 1–8.

63 M. Cohen, M. Gandugliapirovano and J. Kudrnovsky, *Phys. Rev. Lett.*, 1994, **72**, 3222–3225.

64 J. Ireta, M. Galvan, K. Cho and J. Joannopoulos, *J. Am. Chem. Soc.*, 1998, **120**, 9771–9778.

65 F. Aparicio, J. Ireta, A. Rojo, L. Escobar, A. Cedillo and M. Galvan, *J. Phys. Chem. B*, 2003, **107**, 1692–1697.

66 F. Aparicio, N. Gonzalez-Rivas, J. Ireta, A. Rojo, L. I. Escobar, A. Cedillo and M. Galvan, *Int. J. Quantum Chem.*, 2012, **112**, 3618–3623.

67 C. Muñoz Gutierrez, F. Adasme-Carreño, J. Alzate-Morales and J. Ireta, *Phys. Chem. Chem. Phys.*, 2023, **25**, 23885–23893.

This journal is © the Owner Societies 2024

Phys. Chem. Chem. Phys., 2024, **26**, 21468–21475 | **21475**